PERGAMON

International Journal of Solids and Structures 38 (2001) 2149–2159

INTERNATIONAL JOURNAL OF SOLIDS and STRUCTURES

www.elsevier.com/locate/ijsolstr

Vibrations of machines subjected to digital force control

Gábor Stépán *

Department of Applied Mechanics, Technical University of Budapest, H-1521 Budapest, Hungary

Received 9 August 1999; in revised form 19 January 2000

Abstract

When a robot has to interact with the environment, force control of the contact between its actuator and the workpiece may be required. Force control tries to maintain a prescribed contact force. Basic text books often call the attention for the destabilizing digital effects, like sampling, in these systems. In this paper, the stability limits are presented in the parameter space of the sampling time, control gains and mechanical parameters. The least force error and the fastest settling force signal is calculated with simple closed form formulae. These analytical results have a central role in understanding the technical phenomena and in forming the common sense in design work.

Keywords: Stability; Force control; Sampling; Discrete mapping

1. Introduction

The main difficulty in the digital force control of robots is originated in the facts that the force sensor used at the actuator, and also the environment (or workpiece) touched by the actuator, are elastic elements. Moreover, the compliance of the environment is often unknown, it may vary in different tasks, and it is difficult to prepare the control of the robot to handle this problem. The Newcastle robot developed for turbine blade polishing (see Steven and Hewitt, 1987 or Stépán et al., 1990) is a clear example for this, the blade of wing-shaped cross-section has a varying stiffness normal to its surface as the robot actuator slides along it. A great number of other applications could be mentioned where vibration problems occur in similar computer controlled systems (Raibert and Craig, 1981; Chen, 1987; Eppinger and Seering, 1987; Vischer and Khatib, 1990 etc.,).

In order to achieve high accuracy in maintaining the prescribed contact force, high control gains are to be used. In practical, realizations of this force control, however, the robot often loses stability, and starts to oscillate at a relatively low frequency in the range of 2–20 Hz. This frequency looks far smaller than the usual sampling frequency of the digital control. From the mechanical engineering view point, the 0.1–2 kHz sampling frequency applied to a mechanical structure having inertia in the range of 10–100 kg with a first natural frequency in the range of 1–10 Hz, looks 'almost' continuous and negligible. This is not true

* Tel.: +36-1-463-1369; fax: +36-1-463-3471.
E-mail address: stepan@mm.bme.hu (G. Stépán).

0020-7683/01/$ - see front matter
PII: S0020-7683(00)00158-X

(Whitney, 1977, 1985), and simple analytical calculations show that the digital effects have to be taken into account when oscillatory systems are to be controlled, which is the case in force control. Even for a sampling frequency of 10 kHz (i.e. for a sampling time as short as $\tau = 0.1$ ms), the simulation results of Kuno et al. (1988), prove that the dynamics of the digital processor and the mechanical structure should be modeled together since loss of stability may occur for certain parameter values of the mechanical structure and the control system.

The subsequent sections of this paper describe the basic concept of force control in an ideal one degree-of-freedom (DOF) mechanical model, and the stability analysis of a discrete mathematical model of the digital control. Then a stability chart is presented in the plane of mechanical and control parameters, and also the non-linear behavior of the system is forecasted after the loss of stability. The conclusions are derived from the analytical estimations of the least possible force error and that of the exponential power of the fastest settling force signal.

2. Force control

2.1. Continuous model

Fig. 1 presents an ideal one DOF mechanical model of the force control, where m stands for the mass modeling the inertia of the robot, and s denotes the stiffness of the spring which models the elastic force sensor, the elastic environment, or both. This model is often used in basic textbooks to analyze force control (Craig, 1986). The single coordinate y is chosen in a way that the spring is relaxed at $y = 0$. The control force Q is provided by the ideal actuator, and calculated by the digital processor from the contact force error $F_e = F_m - F_d$, which is the difference of the measured and the desired contact force. If the simplest proportional controller is used with the gain $P > 0$ and the contact force is measured via the deformation y of the spring, the control force assumes the form

$$Q = -P(sy - F_d) + sy. \tag{1}$$

Other types of control forces are also mentioned by Craig (1986), and some of them are discussed in Section 5.

If C denotes the constant Coulomb friction force, the equation of motion is as follows:

$$m\ddot{y} + sy = -P(sy - F_d) + sy - C\,\mathrm{sgn}\,\dot{y}. \tag{2}$$

Clearly, the trivial solution $y(t) \equiv y_0 = F_d/s$ satisfies this equation when there is no dry friction, i.e. when $C = 0$. When the perturbation x is introduced by

$$y(t) = y_0 + x(t), \tag{3}$$

the equation of motion,

$$m\ddot{x} + Psx = -C\,\mathrm{sgn}\,\dot{x} \tag{4}$$

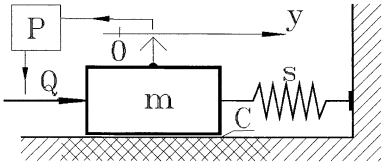

Fig. 1. Mechanical model.

refers to the desired contact force with its trivial zero solution. Clearly, Eq. (4) may have any other constant solution in the interval $[-C/(Ps), C/(Ps)]$, and the corresponding accuracy of the force control can be characterized by the maximum possible force error

$$\Delta F_{\mathrm{e}} = \frac{C}{P}. \tag{5}$$

Thus, the higher the gain is, the less the force error is. Theoretically, there is no upper limit for the gain P, since the zero solution of Eq. (4) is always stable when $C = 0$, moreover, it becomes asymptotically stable in the presence of viscous damping or differential controller. Experiments show, however, that the real system is not stable for high gain P (Stépán et al., 1990). The instability is caused by the digital effects as explained below.

2.2. Discrete model

The digital processor samples the force signal at the time instants $t_j = j\tau$, $j = 0, 1, 2, \ldots$, where τ stands for the sampling time, $f = 1/\tau$ is the sampling frequency. The control force is piecewise constant in the sampling intervals (this effect is also referred to as zero-order holder) and it is calculated from the contact force signal sampled at the beginning of the previous sampling interval:

$$Q(t) \equiv -P(sy(t_j - \tau) - F_{\mathrm{d}}) + sy(t_j - \tau), \quad t \in [t_j, t_j + \tau). \tag{6}$$

When this control force is substituted into the equation of motion (2), the same trivial solution y_0 is obtained, and formula (5) of the contact force accuracy is also the same. However, the stability properties of the equation of motion

$$m\ddot{x}(t) + sx(t) = s(1 - P)x(t_j - \tau), \quad t \in [t_j, t_j + \tau), \ \ j = 0, 1, 2, \ldots \tag{7}$$

for the perturbation variable x are quite different from those of Eq. (4). The stability analysis of the zero solution of Eq. (7) needs somewhat different methods, the well-known Routh–Hurwitz criterion cannot be applied here directly. Still, this stability analysis can be carried out in closed form, and its results can easily be arranged in a stability chart.

To prepare this calculation, let us introduce the angular natural frequency γ and the natural frequency n by

$$\gamma = \sqrt{s/m}, \quad n = \gamma/(2\pi)$$

in the uncontrolled system, and also introduce the dimensionless time T by

$$t = T\tau, \quad t_j = j\tau = T_j\tau \ \Rightarrow \ T_j = j, \ \ j = 0, 1, 2, \ldots$$

The dimensionless time measures the time by the multipliers of the sampling time. If $'$ denotes differentiation with respect to the dimensionless time, and Eq. (7) is divided by the mass m, and also multiplied by the square of the sampling time τ, the mathematical model of the system assumes the form

$$x''(T) + (\gamma\tau)^2 x(T) = (\gamma\tau)^2(1 - P)x(j - 1), \quad T \in [j, j + 1), \quad j = 0, 1, 2, \ldots \tag{8}$$

This equation has a central role in the description of the stability of digital force control.

3. Stability analysis

The stability investigation of the trivial solution of the piecewise continuous system (8) is carried out via the analytical construction of a discrete mapping having the same stability properties.

3.1. Discrete mapping

Since the non-homogeneous ordinary differential equation (8) has a piecewise constant right-hand side, the general solution of Eq. (8) for each sampling interval can be constructed from the sum of the general solution of the homogeneous part and a particular solution of the non-homogeneous part:

$$x(T) = x_h(T) + x_p(T) = B_1 \cos(\gamma\tau T) + B_2 \sin(\gamma\tau T) + (1-P)x(j-1), \quad T \in [j, j+1), \tag{9}$$

while its derivative, the velocity, assumes the form

$$x'(T) = -B_1\gamma\tau \sin(\gamma\tau T) + B_2\gamma\tau \cos(\gamma\tau T), \quad T \in [j, j+1). \tag{10}$$

The coefficients $B_{1,2}$ come from the initial conditions $x(j),\ x'(j)$ for the corresponding jth sampling interval. After the substitution of $T = j$ in Eqs. (9) and (10), the coefficients are obtained from the system of linear algebraic equations

$$\begin{pmatrix} \cos(\gamma\tau T) & \sin(\gamma\tau T) \\ -\gamma\tau \sin(\gamma\tau T) & \gamma\tau \cos(\gamma\tau T) \end{pmatrix} \begin{pmatrix} B_1 \\ B_2 \end{pmatrix} = \begin{pmatrix} x(j) - (1-P)x(j-1) \\ x'(j) \end{pmatrix}$$

in the form

$$B_1 = -(1-P)\cos(\gamma\tau j)x(j-1) + \cos(\gamma\tau j)x(j) - \frac{1}{\gamma\tau}\sin(\gamma\tau j)x'(j),$$

$$B_2 = -(1-P)\sin(\gamma\tau j)x(j-1) + \sin(\gamma\tau j)x(j) + \frac{1}{\gamma\tau}\cos(\gamma\tau j)x'(j).$$

Clearly, the position and the velocity of the block can be calculated at the end of the jth sampling interval by substituting $T = j+1$ into Eq. (9), and also into its derivative (10). After some trigonometric transformation, the substitutions of $B_{1,2}$ result

$$x(j+1) = (1-P)(1-\cos(\gamma\tau))x(j-1) + \cos(\gamma\tau)x(j) + \frac{1}{\gamma\tau}\sin(\gamma\tau)x'(j), \tag{11}$$

$$x'(j+1) = (1-P)\gamma\tau \sin(\gamma\tau)x(j-1) - \gamma\tau \sin(\gamma\tau)x(j) + \cos(\gamma\tau)x'(j). \tag{12}$$

These formulae mean that the position and the velocity of the block at the $(j+1)$th sampling instant can be calculated as a linear combination of the position at the $(j-1)$th and the jth sampling and that of the velocity at the jth sampling. This can also be arranged in matrix form if the 3-D vector

$$\mathbf{z}_j = \begin{pmatrix} x(j-1) \\ x(j) \\ x'(j) \end{pmatrix}, \quad j = 1, 2, \ldots \tag{13}$$

is introduced. The coefficient matrix $\mathbf{A}$ of the 3-D linear mapping

$$\mathbf{z}_{j+1} = \mathbf{A}\mathbf{z}_j \tag{14}$$

can be built up from the coefficients of the corresponding terms of formulae (11) and (12) as follows:

$$\mathbf{A} = \begin{pmatrix} 0 & 1 & 0 \\ (1-P)(1-\cos(\gamma\tau)) & \cos(\gamma\tau) & \frac{1}{\gamma\tau}\sin(\gamma\tau) \\ (1-P)\gamma\tau \sin(\gamma\tau) & -\gamma\tau \sin(\gamma\tau) & \cos(\gamma\tau) \end{pmatrix}. \tag{15}$$

Clearly, the convergence of the 3-D geometrical series (14) is equivalent to the asymptotic stability of the zero solution of Eq. (8), which describes the digital force control.

3.2. Convergence

As explained in basic text books like Kuo (1977), the trivial solution of the linear mapping (14) is asymptotically stable, if and only if all the eigenvalues $\mu_{1,2,3}$ of $\mathbf{A}$ are located within the unit circle (i.e. in the open unit disc) of the complex plane. This is a direct generalization of the well-known convergence criterion for scalar geometrical series. In order to reveal its relation to the stability criteria of continuous systems, consider the difference equation

$$\mathbf{z}(T) = \mathbf{A}\mathbf{z}(T-1), \quad T \in [1, \infty) \tag{16}$$

with the initial function

$$\mathbf{z}(T) = \begin{pmatrix} 0 \\ x(T) \\ x'(T) \end{pmatrix} = \begin{pmatrix} 0 \\ x(0)\cos(\gamma\tau T) + \frac{x'(0)}{\gamma\tau}\sin(\gamma\tau T) \\ -x(0)\gamma\tau\sin(\gamma\tau T) + x'(0)\cos(\gamma\tau T) \end{pmatrix}, \quad T \in [0, 1),$$

where the functions $x(T)$ and $x'(T)$ are the solutions of Eq. (8) with the initial conditions $x(0)$ and $x'(0)$, and with $x(-1) = 0$ on the right-hand side. While this difference equation reproduces the solution of Eq. (8) in the time domain, it also coincides with the discrete mapping (14) when $T = j + 1$ and $j = 0, 1, 2, \ldots$

The stability condition for the difference equation can be constructed via the application of the Laplace transformation for Eq. (16) in the same way as in the case of ordinary differential equations or differential-difference (or delay-differential) equations. For the characteristic roots λ, this procedure gives the same characteristic equation as the substitution of the standard exponential trial solution

$$\mathbf{z}(T) = \mathbf{K}\mathrm{e}^{\lambda T}, \quad \lambda \in C, \quad \mathbf{K} \in R^3 \tag{17}$$

in Eq. (16), that is

$$(\mathbf{I} - \mathbf{A}\mathrm{e}^{-\lambda})\mathbf{K} = 0 \quad \text{and} \quad \mathbf{K} \neq 0 \;\Rightarrow\; \det(\mathbf{I} - \mathbf{A}\mathrm{e}^{-\lambda}) = 0. \tag{18}$$

This characteristic equation has an infinite number of roots λ_k, $k = 1, 2, \ldots$ which are situated along finite number of vertical lines in the complex plane as shown in Fig. 2. As it follows from Eq. (17), the solutions tend to zero if and only if the real parts of all of these characteristic roots are negative. To simplify this calculation, introduce the new complex variable μ by

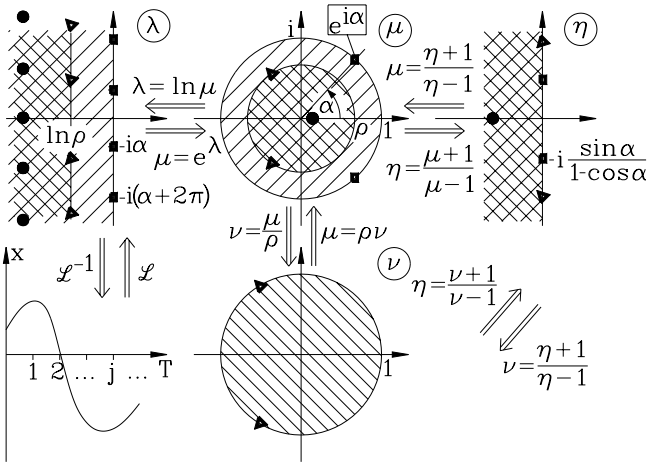

Fig. 2. Transformations for stability and decay analysis.

$$\mu = e^{\lambda} \;\Rightarrow\; \{\mathrm{Re}\,\lambda_k < 0, \quad k = 1,2,\ldots \;\Longleftrightarrow\; |\mu_{1,2,3}| < 1\}. \tag{19}$$

Since the characteristic Eq. (18) gives just the eigenvalues μ of the matrix $\mathbf{A}$, we arrived at the same stability condition for the difference equation (16) as the convergence condition for the discrete mapping (14).

This connection of the two descriptions becomes relevant when the vibration frequencies and exponential decay are calculated in the time domain. For the stability analysis, we follow the calculation of the eigenvalues μ from the characteristic equation (18) after the substitution of Eq. (19)

$$\det(\mu\mathbf{I} - \mathbf{A}) = \sum_{k=0}^{3} b_k \mu^k = 0, \quad \text{where} \quad \begin{pmatrix} b_3 \\ b_2 \\ b_1 \\ b_0 \end{pmatrix} = \begin{pmatrix} 1 \\ -2\cos(\gamma\tau) \\ P + (1-P)\cos(\gamma\tau) \\ -(1-P)(1-\cos(\gamma\tau)) \end{pmatrix}. \tag{20}$$

In order to avoid the tedious algebraic work during the solution of the above third degree equation, the so-called Moebius transformation can be used for the new variable η:

$$\mu = \frac{\eta + 1}{\eta - 1} \;\Rightarrow\; \{|\mu| < 1 \quad \Longleftrightarrow \quad \mathrm{Re}\,\eta < 0\}. \tag{21}$$

This is also shown in Fig. 2 (the inverse of this transformation is identical to itself), and the open unit disc is mapped back to the left half of the complex plane. After the application of this transformation in Eq. (20) and its multiplication by $(\eta - 1)^3$, the equation again becomes third degree polynomial

$$p_3(\eta) = \sum_{k=0}^{3} a_k \eta^k = 0\,. \tag{22}$$

The coefficients a_k can easily be calculated from the coefficients b_k in Eq. (20) as

$$\begin{pmatrix} a_3 \\ a_2 \\ a_1 \\ a_0 \end{pmatrix} = \begin{pmatrix} 1 & 1 & 1 & 1 \\ 3 & 1 & -1 & -3 \\ 3 & -1 & -1 & 3 \\ 1 & -1 & 1 & -1 \end{pmatrix} \begin{pmatrix} b_3 \\ b_2 \\ b_1 \\ b_0 \end{pmatrix} = 2 \begin{pmatrix} P(1-\cos(\gamma\tau)) \\ (3-2P)(1-\cos(\gamma\tau)) \\ P + (2-P)\cos(\gamma\tau) \\ 1 + \cos(\gamma\tau) \end{pmatrix}, \tag{23}$$

where the kth column of the transformation matrix contains the binomial coefficients of $(\eta+1)^{4-k} \times (\eta-1)^{k-1}$, $k = 1,2,3,4$.

As it follows from Eq. (21), it has to be checked whether all the roots $\eta_{1,2,3}$ of p_3 in Eq. (22) are located in the left half of the complex plane. This can, of course, be done by the well-known Routh–Hurwitz criterion (Farkas, 1994) applied to the coefficients in Eq. (22).

The above algorithm for the convergence investigation of any linear discrete mapping like Eq. (14) is given in a densed form in Jury's criterion (Kuo, 1977). The detailed geometrical interpretation of the algorithm also given in Fig. 2 helps the construction of analytical formulae and stability charts, it can also be generalized for frequency and decay analysis within or out of the stability limit, and also gives information on the types of motions bifurcating at the boundaries of stability.

3.3. Stability chart

Note that there are only two parameters in coefficients (23) of the polynomial p_3 in Eq. (22). One is the (dimensionless) gain P of the force control, the other one is the (also dimensionless) $\gamma\tau$ which is proportional to the ratio of the natural frequency n of the uncontrolled system and the sampling frequency f of the control (both measured in Hz):

$$n/f = (\gamma/(2\pi))/(1/\tau) = \gamma\tau/(2\pi). \tag{24}$$

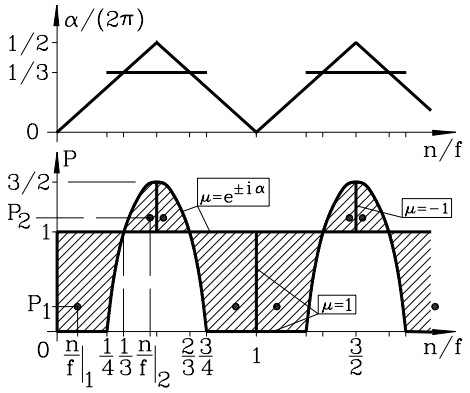

Fig. 3. Stability chart and vibration frequencies.

This gives the possibility to construct 2-D stability charts showing all vibration effects arising in simple force controlled systems in a single parameter plane.

In accordance with the Routh–Hurwitz criterion, the stability of the polynomial p_3 in Eq. (22) is equivalent to the positiveness of all the coefficients a_k, $k = 0, 1, 2, 3$ and also that of the second Hurwitz determinant H_2. Considering formulae (23) of the coefficients, these result the following stability conditions:

$$a_3 > 0 \iff P > 0 \quad \text{and} \quad \gamma\tau \neq 2k\pi, \ \ k = 0, 1, \ldots, \tag{25}$$

$$a_2 > 0 \iff P < \tfrac{3}{2} \quad \text{and} \quad \gamma\tau \neq 2k\pi, \ \ k = 0, 1, \ldots, \tag{26}$$

$$a_1 > 0 \iff P > -2\frac{\cos(\gamma\tau)}{1 - \cos(\gamma\tau)}, \tag{27}$$

$$a_0 > 0 \iff \gamma\tau \neq (2k+1)\pi, \quad k = 0, 1, \ldots, \tag{28}$$

$$H_2 = a_2a_1 - a_3a_0 > 0 \iff 1 > P > -3\frac{\cos(\gamma\tau)}{1 - \cos(\gamma\tau)} \quad \text{or} \quad 1 < P < -3\frac{\cos(\gamma\tau)}{1 - \cos(\gamma\tau)}. \tag{29}$$

The corresponding domains of stability are shaded in Fig. 3.

This chart has a surprising structure, and relevant conclusions can be drawn from it, which are essential for designers and experimentalists who detect different kinds of vibration phenomena in these structures. They are discussed in detail in Section 5. Note the main difference between the stability of the frictionless ($C = 0$) continuous model (4) and that of the more realistic digital model (8): without digital effects, the desired contact force is stable (but not asymptotically stable) for any positive gain P, while the digital effects may result asymptotic stability in very limited distinct parameter domains only where the gain has to be less than $3/2$ and the sampling and the natural frequencies have to be tuned properly.

4. Dynamic properties

In the stability chart of Fig. 3, the critical characteristic roots are also presented at the stability limit. With their help the kind of bifurcating motions can be identified, the frequencies of vibrations occurring can be estimated, and also the strongest exponential decay, the fastest settling signal, can be calculated.

4.1. Bifurcations

As can be shown generally, only the coefficients of the highest and lowest degree terms and the Hurwitz determinant provide the borders of stability, that is conditions (26) and (27) are redundant in this respect.

When $a_3 = 0$, there is an eigenvalue μ of the linear mapping (14) at $+1$ on the unit circle. The physical meaning of this bifurcation at $P = 0$ is obvious: the desired contact force is unstable for negative gains (the control works 'just in the wrong way'), and other stable equilibria may show up around it, depending on the exact structure of the non-linearity in the system. If it is symmetric, a supercritical pitchfork bifurcation is the most typical case here. The physical interpretation of the degenerate bifurcations along the vertical lines $n/f = 1, 2, \ldots$, i.e. at $\gamma\tau = 2\pi, 4\pi, \ldots$, is more difficult and has little importance since they disappear in the presence of the slightest viscous damping in the system. However, a lot of additional calculations are required to prove this.

When $a_0 = 0$, another kind of degenerate bifurcation occurs along $n/f = 1/2, 3/2, \ldots$, i.e. at $\gamma\tau = \pi, 3\pi, \ldots$, where the linear mapping (14) has eigenvalues at -1 on the unit circle. This bifurcation, however, exhibits the period doubling (or flip) bifurcation (Guckenheimer and Holmes, 1986) in the presence of perturbation via slight viscous damping. The corresponding vibration frequency is just the half of the sampling frequency; in other words, its period of oscillation is the double of the sampling time τ. These frequency values are shown at the corresponding peaks of the vibration frequency curves above the stability chart in Fig. 3.

Along the further stability limits there are complex conjugate roots on the unit circle in the form $\mu_{1,2} = \cos\alpha \pm \mathrm{i}\sin\alpha$, $\alpha \in (0, \pi)$ (see them and their transformed versions also in Fig. 2). If the corresponding discrete solutions are transformed back into the dimensionless time domain of T by $\lambda = \ln\mu$, oscillatory solutions are obtained with the dimensionless angular frequencies $\alpha \pm 2k\pi$. Actually, there are infinitely many of these, but the lowest α is experienced the strongest in the spectrum of oscillations in practice, the existence of the higher order ones refer only to the fact that the motion is a combined series of shifted piecewise harmonic oscillations as calculated in Eqs. (9) and (10), so they cannot be expressed as a finite sum of harmonic components. This bifurcation is still analogous to the Hopf bifurcation (or flutter) in the time domain.

4.2. Vibration frequencies

In the case of the Hopf bifurcation $H_2 = 0$, the lowest angular frequencies in the oscillation at the loss of stability can be calculated in closed form. There are two cases as shown by formula (29) when the roots of Eqs. (22) and (20) can be calculated easily:

$$P = 1 \Rightarrow \eta_{1,2} = \mp\mathrm{i}\frac{\sin(\gamma\tau)}{1-\cos(\gamma\tau)} \Rightarrow \mu_{1,2} = \mathrm{e}^{\pm\mathrm{i}\gamma\tau} \Rightarrow$$
$$\alpha = (-1)^k(\gamma\tau - k\pi), \quad \gamma\tau \in (k\pi, (k+1)\pi), \quad k = 0, 1, \ldots, \tag{30}$$

or

$$P = -3\frac{\cos(\gamma\tau)}{1-\cos(\gamma\tau)} \;\Rightarrow\; \eta_{1,2} = \mp\mathrm{i}\frac{1}{\sqrt{3}} \;\Rightarrow\; \mu_{1,2} = -\frac{1}{2} + \mathrm{i}\frac{\sqrt{3}}{2} \;\Rightarrow\; \alpha = \frac{2\pi}{3}. \tag{31}$$

The corresponding frequencies $\alpha/(2\pi)$ are presented above the stability limits in Fig. 3. The frequencies in the original time domain $t = T\tau$ are $\alpha/(2\pi\tau)$ in Hz. Clearly, these frequencies may be far smaller than the sampling frequency $f = 1/\tau$ and cannot be greater than the half of it.

4.3. Exponential decay

There are several view points the engineer should consider during the design of a force-controlled structure. One is the minimum force error, which requires high gains. The highest gain 3/2 can be achieved at the limit of stability only, which means that the system will settle slowly, with high accuracy, though. However, some applications may require fast settling, short transients, as opposed to high accuracy.

The relation of the difference equation model (16) and the discrete mapping (14) shows that the estimate,

$$|\mu_{1,2,3}| < \rho(\leqslant 1) \;\Rightarrow\; \mathrm{Re}\,\lambda_k < \ln\rho,\ k = 1,2,\ldots \;\Rightarrow\; \exists K > 0, \quad \forall T > 0\colon |x(T)| < K\mathrm{e}^{T\ln\rho}, \tag{32}$$

is true (see also Fig. 2). This means that the smaller the spectral radius ρ of the eigenvalues $\mu_{1,2,3}$ is, the stronger the exponential decay of the signal is. With the help of the new complex variable v and the transformation $\mu = \rho v$, the domains of stability can be shrunk to identify those smaller parameter regions in the $(P, n/f)$ parameter plane, where the vibration signal x settles with an exponential power less than $\ln\rho(\leqslant 0)$. To do this, the same Moebius transformation has to be repeated between v and η as before in Eq. (21) (see also in Fig. 2). Thus,

$$\mu = \rho v, \quad v = \frac{\eta+1}{\eta-1} \;\Rightarrow\; \{|\mu| < \rho \iff |v| < 1 \iff \mathrm{Re}\,\eta < 0\}, \tag{33}$$

and the same algorithm results the polynomial p_3 in Eq. (22) with the following coefficients:

$$\begin{pmatrix} a_3 \\ a_2 \\ a_1 \\ a_0 \end{pmatrix} = \begin{pmatrix} 1 & 1 & 1 & 1 \\ 3 & 1 & -1 & -3 \\ 3 & -1 & -1 & 3 \\ 1 & -1 & 1 & -1 \end{pmatrix} \begin{pmatrix} \rho^3 b_3 \\ \rho^2 b_2 \\ \rho b_1 \\ b_0 \end{pmatrix}$$
$$= \begin{pmatrix} \rho^3 - 2\rho^2\cos(\gamma\tau) + \rho(P + (1-P)\cos(\gamma\tau)) - (1-P)(1-\cos(\gamma\tau)) \\ 3\rho^3 - 2\rho^2\cos(\gamma\tau) - \rho(P + (1-P)\cos(\gamma\tau)) + 3(1-P)(1-\cos(\gamma\tau)) \\ 3\rho^3 + 2\rho^2\cos(\gamma\tau) - \rho(P + (1-P)\cos(\gamma\tau)) - 3(1-P)(1-\cos(\gamma\tau)) \\ \rho^3 + 2\rho^2\cos(\gamma\tau) + \rho(P + (1-P)\cos(\gamma\tau)) + (1-P)(1-\cos(\gamma\tau)) \end{pmatrix}. \tag{34}$$

For certain fixed values of ρ, the domains in question can be plotted by the use of the Routh–Hurwitz criterion in the same way as in case of the stability chart.

We can find, however, in closed form that critical value $\rho_{\min}$ of the radius where the domains shrink to a point. There are two possibilities for this. In the domain $\gamma\tau \in (0, 2\pi/3)$, i.e. for $n/f \in (0, 1/3)$, the domain disappears when $a_3 = a_2 = a_1 = 0$ (which yields also $H_2 = a_2a_1 - a_3a_0 = 0$). This means three equations for the three unknowns P, $\gamma\tau$, and ρ. The explicit elimination of P and $\cos(\gamma\tau)$ leaves the algebraic equation

$$\rho^3 + 3\rho^2 - 1 = 0. \tag{35}$$

Its only solution in the interval [0,1] and also the corresponding other parameters assume the form

$$\rho_{\min,1} = -1 + 2\cos\frac{2\pi}{9} = 0.532, \quad (\gamma\tau)_1 = 0.647, \quad (n/f)_1 = 0.103, \quad P_1 = 0.254. \tag{36}$$

There is another point where the exponential decay boundaries disappear; it is at $\gamma\tau \in (2\pi/3, \pi)$, i.e. at $n/f \in (1/3, 1/2)$. Now, the system of the three equations $a_2 = a_1 = a_0 = 0$ (yielding $H_2 = 0$ again) leads to

$$\rho^3 - 3\rho^2 + 1 = 0 \tag{37}$$

having the solutions

$$\rho_{\min,2} = 1 + 2\cos\frac{5\pi}{9} = 0.653, \quad (\gamma\tau)_2 = 2.936, \quad (n/f)_2 = 0.467, \quad P_2 = 1.141. \tag{38}$$

These points are also presented in the stability chart of Fig. 3.

When decision has to be made which point is better in practice, the dilemma of the designer is clear: either use parameter point 1 with force error (5) and decay (32) given as

$$\Delta F_e = C/P_1 = 3.937C, \quad |x(t)| \leqslant K e^{t \ln \rho_{\min,1}/\tau} = K e^{-0.631 t/\tau} \tag{39}$$

or use parameter point 2 with

$$\Delta F_e = C/P_2 = 0.876C, \quad |x(t)| \leqslant K e^{t \ln \rho_{\min,2}/\tau} = K e^{-0.427 t/\tau}, \tag{40}$$

i.e. either the error is high and settling is fast, or the error is small but settling is slow. In the extreme case, when the force error reaches its minimum at $2C/3$, the system already starts losing stability with the value $\rho = 1,\ \ln \rho = 0$.

5. Conclusions

In the case of computer controlled elastic structures, the digital implementation of force control may result in unexpected stability behavior and vibrations. These problems occur even for very high values of sampling frequencies which otherwise result 'almost continuous' signals for the mechanical structure.

The stability chart in Fig. 3 of digital force control shows that the stability limit for the maximum proportional control gain strongly depends on the ratio of the natural frequency of the uncontrolled system and the sampling frequency of the digital control. It is not the shortest sampling time, which provides the highest gain within the stability limit, and this calls the attention for the proper tuning of the sampling frequency. Since the highest proportional gain is $3/2$, the best force accuracy is $2C/3$, i.e., the force error cannot be guaranteed to be below 66% of the dry friction in a structure with negligible viscous damping.

Note also that Craig (1986) suggests the control force in the form

$$Q = -P(sy - F_d) + F_d \tag{41}$$

instead of Eq. (1). This seems to result in a smaller force error

$$\Delta F_e = \frac{C}{P+1} \tag{42}$$

than the one given in Eq. (5). Still, the digital implementation of this slightly different control will result the same force error since the repeated calculations for Eq. (41) show that the maximum possible gain P within the stability limit is 1/2 only, the whole stability chart in Fig. 3 is shifted downwards by 1. Thus, there is no practical difference between the control (1) and (41).

Although all kinds of possible bifurcations of discrete systems can be found along the stability limits, the typical one is the flutter (or Hopf bifurcation) in practical cases. The vibration frequencies after the loss of stability may be in the range of 0–50% of the sampling frequency (see the upper part of Fig. 3). This frequency may be so small (even smaller than the natural frequencies of the mechanical structure itself) that the experimentalist would never suspect the high frequency digital effects as a cause of the problem.

The exponential decay of the signal cannot be better than $\exp(-0.631 t/\tau)$ as shown in Eq. (39), where the short sampling delay τ results fast settling, of course. However, at this parameter point (Fig. 3) the force error is quite high, almost four times the Coulomb friction in the structure. The stability chart of Fig. 3 is a good tool to develop physical sense of these digitally controlled structures, and the designer can optimize between the view points of least error and fastest settling. The method described here can be used also for systems with viscous damping or with more degrees of freedom, although, the calculations cannot be repeated in closed form anymore, and the influence of the parameters cannot be represented geometrically in simple stability charts.

Acknowledgements

This research was supported by the Hungarian Scientific Research Foundation under grant No. OTKA T030762 and the Ministry of Culture and Education under grant No. FKFP 0380/97.

References

Craig, J.J., 1986. Introduction to Robotics Mechanics and Control. Addison-Wesley, Reading, MA.

Chen, Y., 1987. Frequency response of discrete-time robot systems. In: Proceedings of IEEE Conference on Robotics and Automation. Raleigh, pp. 464–472.

Eppinger, D.S., Seering, W.P., 1987. Understanding bandwidth limitations in robot force control. Proceedings IEEE Conference on Robotics and Automation. Raleigh, pp. 904–909.

Farkas, M., 1994. Periodic Motions. Springer, New York.

Guckenheimer, J., Holmes, P., 1986. Nonlinear Oscillations, Dynamical Systems, and Bifurcation of Vector Fields. Springer, New York.

Kuno, T., Koide, M., Mimura, N., Miyaguchi, H., 1988. Simulation analysis for force control six-joint manipulator. In: Proceedings of fourth International Symposium on Robotics Research. Cambridge, pp. 207–216.

Kuo, B.C., 1977. Digital Control Systems. SRL Publishing Company, Champaign, Illinois.

Raibert, M.H., Craig, J.J., 1981. Hybrid position/force control for computer controlled manipulators. ASME Journal of Dynamic Systems, Measurement and Control 102, 125–133.

Stépán, G., Steven, A., Maunder, L., 1990. Design principles of digitally controlled robots. Mechanism and Machine Theory 25, 515–527.

Steven, A., Hewit, J.R., 1987. Hybrid position and force control applied to robotic polishing of turbine blading. In: Proceedings of ICAR'87 third Conference on Advanced Robotics. Versailles, 493–502.

Vischer, D., Khatib, O., 1990. Design and Development of Torque-controlled Joints. In: Hayward, V., Khatib, O. (Eds.), Experimental Robotics I. Springer, Berlin.

Whitney, D.E., 1977. Force feedback control of manipulator fine motions. ASME Journal of Dynamic Systems, Measurement and Control 98, 91–97.

Whitney, D.E., 1985. Historical perspective and state of the art in robot force control. International Journal of Robotics Research 6, 3–14.